Role of Phenylalanine B10 in Plant Nonsymbiotic Hemoglobins[†,‡]

Benoit J. Smagghe,[§,||] Suman Kundu,[⊥] Julie A. Hoy, Puspita Halder, Theodore R. Weiland, Andrea Savage, Anand Venugopal, Matthew Goodman, Scott Premer, and Mark S. Hargrove*[,§]

Department of Biochemistry, Biophysics, and Molecular Biology, Iowa State University, Ames, Iowa 50011, Université des Sciences et Technologies de Lille, UMR USTL/INRA1281 SADV "Stress abiotiques et diffrenciation des végétaux cultivés", ERT 1016, 59655 Villeneuve d'Ascq, France, and School of Biotechnology, Banaras Hindu University, Varanasi-221005, India.

Received April 13, 2006; Revised Manuscript Received June 6, 2006

ABSTRACT: All plants contain an unusual class of hemoglobins that display bis-histidyl coordination yet are able to bind exogenous ligands such as oxygen. Structurally homologous hexacoordinate hemoglobins (hxHbs) are also found in animals (neuroglobin and cytoglobin) and some cyanobacteria, where they are thought to play a role in free radical scavenging or ligand sensing. The plant hxHbs can be distinguished from the others because they are only weakly hexcacoordinate in the ferrous state, yet no structural mechanism for regulating hexacoordination has been articulated to account for this behavior. Plant hxHbs contain a conserved Phe at position B10 (Phe^{B10}), which is near the reversibly coordinated distal His^{E7}. We have investigated the effects of Phe^{B10} mutation on kinetic and equilibrium constants for hexacoordination and exogenous ligand binding in the ferrous and ferric oxidation states. Kinetic and equilibrium constants for hexacoordination and ligand binding along with CO-FTIR spectroscopy, midpoint reduction potentials, and the crystal structures of two key mutant proteins (F40W and F40L) reveal that Phe^{B10} is an important regulatory element in hexacoordination. We show that Phe at this position is the only amino acid that facilitates stable oxygen binding to the ferrous Hb and the only one that promotes ligand binding in the ferric oxidation states. This work presents a structural mechanism for regulating reversible intramolecular coordination in plant hxHbs.

Hemoglobins (Hbs) are multi-functional globular proteins that use a heme prosthetic group in their activities. The chemical behavior of heme is dominated by its coordination to the protein scaffold and by the amino acid side chains that line the binding pocket. While coordination in Hbs is always via a His side chain, the structure of the rest of the heme pocket is quite variable. As a result, Hbs have a wide range of ligand affinities and redox properties that are required for their individual physiological functions.

In mammalian oxygen transport proteins, the His^{F8} side chain coordinates the heme group on the proximal side (*1*). His^{E7} is on the distal side of the porphyrin and does not coordinate the heme iron but interacts with the bound ligand to create appropriate affinity and rate constants for facilitating oxygen diffusion (*2*). Another conserved amino acid in the ligand binding pocket is Leu^{B10}, which does not directly interact with bound ligands but influences binding by orienting His^{E7} for hydrogen bonding with oxygen (*3*, *4*) (Figure 1). In plant oxygen transport proteins (leghemoglobins), the side chain at position B10 also tunes the influence of His^{E7} on bound oxygen to control affinity (*5*, *6*).

Many other Hbs are found in plants, animals, and bacteria for which physiological functions have not yet been assigned with any real confidence (*7*−*9*). In many of these proteins, the amino acid at position B10 has a direct role in ligand binding regulation. These Hbs include the truncated Hbs (*10*), those from the parasitic nematode *Ascaris suum* (*11*), the mollusk *Lucina pectinata* (HbII) (*12*), and the Hb domains of bacterial and yeast flavohemoglobins (*13*). Although this large and diverse group of Hbs displays considerable variation in their structures and functions, they have in common the combination of Tyr^{B10}/Gln^{E7} in their heme pockets (an example is *Ascaris* Hb in Figure 1). As a result of direct stabilization of bound oxygen by Tyr^{B10}, most of these proteins have oxygen affinities that are too high for transport, but the Tyr^{B10}/Gln^{E7} combination has proven to be effective for scavenging and detoxification reactions such as NO dioxygenation (*14*).

Another group of the Hbs known as hexacoordinate Hbs (hxHbs) are found in all plants and animals (*9*). In the absence of exogenous ligands, both His^{F8} and His^{E7} coordinate the heme iron in a manner similar to that of cytochrome *b5*. However, unlike cytochrome *b5*, the side chain of His^{E7}

[†] This work was made possible by the National Institutes of Health Award R01-GM065948, support from the Iowa State University Plant Sciences Institute, by a 'Contrat Plan-Etat-Région' to the Laboratoire "Stress abiotiques et diffrenciation des végétaux cultivés", and by a doctoral fellowship of the 'Conseil Régional du Nord-Pas de Calais' to B.J.S.

[‡] The atomic coordinates for the crystal structure of riceF40L and riceF40W are available in the Protein Data Bank at Research Collaboratory for Structural Bioinformatics under pdb numbers 2GNV and 2GNW, respectively.

* To whom correspondence should be addressed. Tel: 515-294-2616. Fax: 515-294-0520. E-mail: msh@iastate.edu.

[§] Iowa State University.

[||] Université des Sciences et Technologies de Lille.

[⊥] Banaras Hindu University.

[1] F8 denotes a primary structure position with structural homology to myoglobin where F stands for the F helix, and 8 stands for the eighth amino acid of the helix.

10.1021/bi060716s CCC: $33.50
Published on Web 07/22/2006

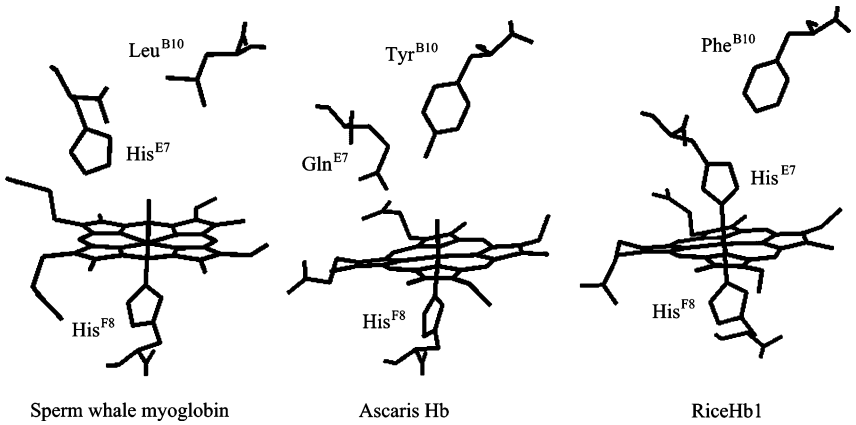

FIGURE 1: B10, E7, and F8 amino acids in the heme pockets of sperm whale myoglobin (2MBW), *Ascaris* Hb (1ASH), and riceHb1 (1D8U).

can be displaced by exogenous ligands in both the ferric and ferrous forms. The biological function and purpose of hexacoordination are not yet known, nor is the chemical mechanism facilitating displaceable coordination.

In plant hxHbs, Phe^{B10} is conserved and located very close to His^{E7} (*15*) (Figure 1). For this reason, we hypothesize that Phe^{B10} might confer an important function to these proteins by influencing hexacoordination. Here, we present a combination of ligand-binding measurements in both the ferrous and ferric heme oxidation states, potentiometric redox titrations, visible and IR spectroscopy, and X-ray crystallography to measure the effects of Phe^{B10} substitution on hexacoordination and ligand binding in a hxHb from rice (riceHb1). Our results demonstrate that the Phe^{B10} is the only amino acid that allows the formation of a stable oxyferrous complex and the ability to bind ligands in the ferric oxidation state with high affinity.

METHODS

Protein Production. RiceHb1 and Phe^{B10} (amino acid 40 in the primary structure) mutant proteins were expressed as described previously (*16*) using the host strain BL21 Star DE3 (Invitrogen). Purification was achieved using a three step process described earlier (*17*). Absorbance spectra were collected with a Varian Cary-Bio spectrophotometer at room temperature in a 0.1 M potassium phosphate buffer at pH 7.0. The proteins were first oxidized with a slight excess of ferricyanide and then run over a G25 column. Sodium dithionite was added to record the deoxy ferrous spectra in Figure 4.

Ligand Binding and Autoxidation Experiments. Rate constants for CO binding (k'_{CO}) and for hexacoordination (k_{H2} and k_{-H2}) in ferrous Hbs were measured as described by Smagghe et al. (*16*). In summary, flash photolysis was used to measure k'_{CO} from the [CO] dependence of rebinding (*18*). k_{H2} and k_{-H2} were measured from the concentration dependence of CO binding following rapid mixing. Time courses for CO binding initiated by rapid mixing follow eq 1:

$$\Delta A_{obs} = -A_T(F_P e^{-k'_{CO}[CO]^* t} + F_H e^{-k'_{obs,CO}[CO]^* t}) \quad (1)$$

In this equation, ΔA_{obs} is the observed time course for binding, k'_{CO} is the bimolecular rate constant for CO binding to the pentacoordinate complex (Hb_{P2} in Scheme 1),

Scheme 1

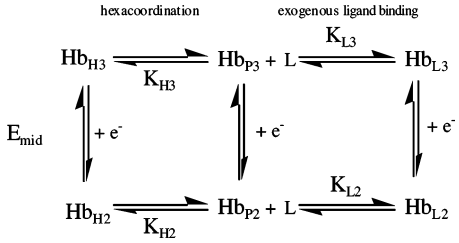

and $k'_{obs,CO}$ is the observed rate constant for binding following mixing as described by eq 2. F_P and F_H are the fractions of protein in the penta and hexacoordinate states, and ΔA_T is the total change in absorbance expected for the reaction (calculated independently from ligand-free and ligand-bound absorbance spectra).

$$k_{obs,CO} = \frac{k_{-H2}k'_{CO}[CO]}{k_{H2} + k_{-H2} + k'_{CO}[CO]} \quad (2)$$

Eq 2 correlates the observed rate constant for CO binding to the hexacoordinate fraction (or rapid equilibrium between hexa and pentacoordinate states) following rapid mixing. k_{H2} and k_{-H2} are the rate constants for association and dissociation of the His^{E7} side chain.

Rapid mixing experiments measuring O_2 dissociation rate constants have been described previously (*19*) and were conducted with a BioLogic SFM 400 stopped-flow reactor coupled to a MOS 250 spectrophotometer. The O_2-bound proteins were prepared as previously described (*20*) and collected in syringes containing 262 μM O_2. A CO solution (1 mM + 100 μM sodium dithionite) was used as the displacing ligand.

Two types of experiments were conducted to measure rate constants for autoxidation. For slower reactions (wild-type riceHb1 and F40W), a Varian Cary 50 spectrophotometer was used to monitor the oxidation of oxyferrous samples as described by Brantley et al. (*4*). For fast reactions ($k_{ox} > 10$ h^{-1}), the Brantley method was performed in the stopped flow reactor. The four syringes of the apparatus were used to create the oxygenated sample by first mixing a ferric protein with a stoichiometric concentration of sodium dithionite (as measured by its absorbance at 315 nm (*21*)), allowing time for reduction (typically 20 s), and then mixing against a saturated oxygen solution to generate the oxyferrous com-

plex. These spectra were collected over time to monitor oxidation. As a control, this procedure was used to measure the autoxidation rate constant for sperm whale myoglobin and provided the same value obtained by traditional methods (*4*).

Azide binding was measured by an equilibrium titration of 3 μM Hbs with sodium azide in 0.1 M potassium phosphate at pH 7.0, using a Varian Cary 50 spectrophotometer. The association equilibrium constants ($K_{obs,azide}$) for each protein (Table 2) were extracted using the following equation:

$$F_B = \frac{K_{obs,azide}[azide]}{1 + K_{obs,azide}[azide]} \quad (3)$$

FTIR Spectroscopy. Samples of CO-bound Hbs were prepared as described previously (*6*). Briefly, the proteins (2−3 mM) were reduced with a dithionite solution in an Eppendorf tube equilibrated with CO. The protein sample was added to a BioCell cuvette (5 mm thickness × 50 mm diameter, separated by a 40 μm spacer; BioTools, Inc.) and spectra acquired with a Nicolet Nexus 470 FTIR spectrometer (Nicolet Instrument Corp., Wisconsin) coupled to an external liquid-nitrogen cooled MCT detector. Spectra were recorded at 1 cm^{-1} resolution in the region 1800−2100 cm^{-1}. Up to 128 interferograms were collected for all samples and their corresponding deoxy protein controls. The final IR spectra were corrected for buffer background by subtraction of the sample and control data.

Spectroelectrochemistry. Potentiometric titrations were performed using an Ocean-Optics UV−Vis spectrophotometer (USB 2000) and an Oakton pH-mV meter (pH 1100 series) adopting the method described by Altuve et al. (*22*) and monitoring the absorbance change associated with conversion of the ferric protein to the deoxyferrous. A standard saturated calomel electrode (SCE) was used as a reference electrode, and a platinum electrode was used as a working electrode for all measurements. Reduction potentials and E_{obs} values are reported with reference to a standard hydrogen electrode (SHE).

Titrations of 10 μM Hb were carried out at 25 °C in argon saturated 0.1 M potassium phosphate at pH 7.0. Ferric proteins were titrated stepwise with a solution of sodium dithionite (40 mM) previously sparged with argon. Reduction was monitored by recording the absorbance spectrum in the visible region (500−700 nm), and the corresponding cell potential was noted for every addition of dithionite after the attainment of equilibrium. A group of redox mediators were used to buffer the entire potential range starting from +160 to −440 mV. Their standard reduction potential versus SHE are 1,2-naphthoquinone E_{mid} = +157 mV), toluylene blue (E_{mid} = +115 mV), duroquinone (E_{mid} = +5 mV), hexaammineruthenium (III) chloride (E_{mid} = −50 mV), pentaaminechlororuthenium (III) chloride (E_{mid} = −40 mV), 5,8-dihydroxy-1,4-naphthoquinone (E_{mid} = −50 mV), 2,5-dihydroxy-1−4 benzoquinone (E_{mid} = −60 mV), 2-hydroxy-1,4-naphthoquinone (E_{mid} = −137 mV), anthraquinone-1,5-disulfonic acid (E_{mid} = −175 mV), 9,10-anthraquinone-2,6-disulfonic acid (E_{mid} = −184 mV), and methyl viologen (E_{mid} = −440 mV).

Midpoint potentials were extracted from the change in absorbance by the following general equation.

$$F_{reduced} = \frac{e^{-(nF(E_{obs}-E_{mid})/RT)}}{1 + e^{-(nF(E_{obs}-E_{mid})/RT)}} \quad (4)$$

$F_{reduced}$ is the normalized change in absorbance at 557 nm, E_{obs} is the observed cell potential, and E_{mid} is the fitted midpoint potential following eq 4.

X-ray Crystallography. The purified proteins were oxidized with a molar excess of potassium ferricyanide, desalted on a Sephadex G-25 column in 0.01 M potassium phosphate at pH 7.0, concentrated to ∼3 mM, and stored at −80 °C until use. Crystal growth was achieved by hanging-drop vapor diffusion. Drops were produced by mixing 2 μL of 3 mM protein with 2 μL of well buffer containing 1.9 M ammonium phosphate, 20% sucrose, and 3% dioxane at pH 7.0. Single crystals grew overnight for F40L and within a week for F40W, both at room temperature.

Diffraction data were collected at 100 K on a Rigaku/MSC home source generator and processed using d*TREK (*23*). Molecular replacement was performed using CNS (*24*) and the structure of riceHb1 (1D8U.pdb) as the starting model. The refinement of F40L was performed using both CNS and CCP4 (*25*) with manual rebuilding in O (*26*). The final model is a dimer containing a total of 319 aminoacids (residues A1−7 and B1−10 were left out because of the lack of density and to improve statistics) and 222 water molecules, with R = 20.3%, R_{free} = 24.7%, and 99.8% completeness from 20 to 2.3 Å. The crystals of F40W were twinned with twinning fraction 0.47. The twinning scripts in CNS were used to refine the structure. The final model is a dimer containing a total of 330 amino acids and 97 waters, with R = 17.5%, R_{free} = 20.4%, and 97.5% completeness from 20 to 2.4 Å.

RESULTS

As diagramed in Scheme 1, the hexacoordinate forms of the ferrous (Fe^{2+}) and ferric (Fe^{3+}) Hb (Hb_{H2} and Hb_{H3}, respectively) can bind exogenous ligands (L) following the conversion to the pentacoordinate state (Hb_P). The association equilibrium constants for hexacoordination are K_{H2} and K_{H3} for the ferrous and ferric oxidation states, and the association equilibrium constants for exogenous ligand binding to the respective pentacoordinate forms are K_{L2} and K_{L3}. The reduction of the ferric protein (Hb_3) can be described by a midpoint reduction potential (E_{mid}), which is thermodynamically linked to all binding described in the scheme (*27*).

Most reports of ligand binding to hxHbs have investigated only the ferrous oxidation state (*16*, 28−30). The values of K_{H2} range from 10^3 to 0.5, with plant hxHbs displaying lower values and significant fractions of the pentacoordinate heme (Hb_{P2}) (*16*). Our first goal was to measure the results of Phe^{B10} substitution on hexacoordination and ligand binding in the ferrous form to determine if this side chain plays a role in regulating K_{H2}.

Ligand Binding and Hexacoordination in the Ferrous Oxidation State

Hexacoordination and CO Binding. A combination of flash photolysis and rapid mixing experiments were employed to measure rate and affinity constants for hexacoordination in the ferrous state of wild-type riceHb1 and five Phe^{B10} mutant proteins. Rate constants for bimolecular CO binding (k'_{CO};

Table 1: Ferrous Reactions and Autoxidation

protein	k_{H2} (s^{-1})	k_{-H2} (s^{-1})	K_{H2}	$k'_{CO,pent}$ ($\mu M^{-1} s^{-1}$)	k_{O2} (s^{-1})	k_{ox} (h^{-1})	ν_{CO} (cm^{-1})
H73L				400	51	0.9	1958
F40G	260	8	33	5	n.d	60	1962
F40A	200	4.3	47	9	n.d.	20	1938
F40L	440	10	44	9	n.d.	50	1937
Phe^{40} (wt)	75	40	1.9	7	0.04	0.08	1926
F40Y	200	10	20	5	n.d.	>100	1964
F40W	430	28	15	0.9	0.06	8	1933

Table 1) as measured by flash photolysis (*18*) show very little variation with the exception of F40W (these data are not shown for the proteins in Figure 2 but are shown for the F40W protein in Figure 3). Figure 2 shows time courses for CO binding initiated by rapid mixing. This experiment is described in detail elsewhere (*16*), and can be summarized as follows: prior to mixing with CO, the ferrous hxHb is at equilibrium with respect to the Hb_{H2} and Hb_{P2} states. If equilibrium is rapid with respect to CO binding or if the fraction of pentacoordinate protein (F_P) ~0, a single rate is observed that obeys eq 2 (which is equivalent to eq 1 with $F_P = 0$). If equilibration is slow compared to CO binding and F_P is substantial, then two rates are observed according to eq 1. Frequently (as exemplified by wild-type riceHb1), the bimolecular reaction is faster than the stopped flow dead time, and the amplitude lost in reaction is proportional to F_p (*16*). Therefore, the loss of amplitude indicates substantial F_P (and lower values of K_{H2}). This experiment, in combination with k'_{CO} from flash photolysis, provides k_{-H2}, k_{H2}, and K_{H2} for each protein (Table 1).

Figure 2 shows time courses that have been normalized to the expected ΔAbs value for the reaction. We have previously demonstrated that wild-type riceHb1 has a value of K_{H2} close to 2 (*16*). The fractions of Hb_H and Hb_P resulting from K_H (for either oxidation state) can be calculated as $F_H = K_H/(1 + K_H)$ and $F_P = 1 - F_H$. The appreciable F_P associated with wild-type riceHb1 in combination with rapid k'_{CO} predicts the loss in reaction amplitude as [CO] increases, which is clear in Figure 2A. The reaction time courses for the same CO concentrations are shown in Figures 2B−E for the F40G, F40A, F40L, and F40Y mutant proteins. For each mutant protein, no loss in reaction amplitude is observed, indicating that K_{H2} is much larger than that for the wild-type protein.

These experiments also provide k_{-H2} as the asymptote of the $k'_{CO,obs}$ rate constants (eq 2) (*16*). These values for each protein are plotted in the inset for each respective set of time courses. The fits of each inset plot to eq 2 (with k_{-H2} fixed as the asymptote) yield k_{H2}. The values of k_{H2} and k_{-H2} (Table 1) provide additional support to the conclusion that each Phe^{40} substitution increases K_{H2} compared to that of the wild-type protein.

The behavior of the F40W mutant protein is unique and is, therefore, presented in expanded detail in Figure 3. An example of a time course for CO binding following flash photolysis is shown in Figure 3A. It is markedly biphasic, with a fast phase that varies with [CO] (Figure 3B) and a slow phase of 28 s^{-1} that is independent of [CO]. The linear fit of Figure 3B provides k'_{CO} as 0.9 $\mu M^{-1} s^{-1}$, a value much smaller than that of wild-type riceHb1 or any of the other Phe^{B10} mutant proteins. Rapid mixing time courses show the

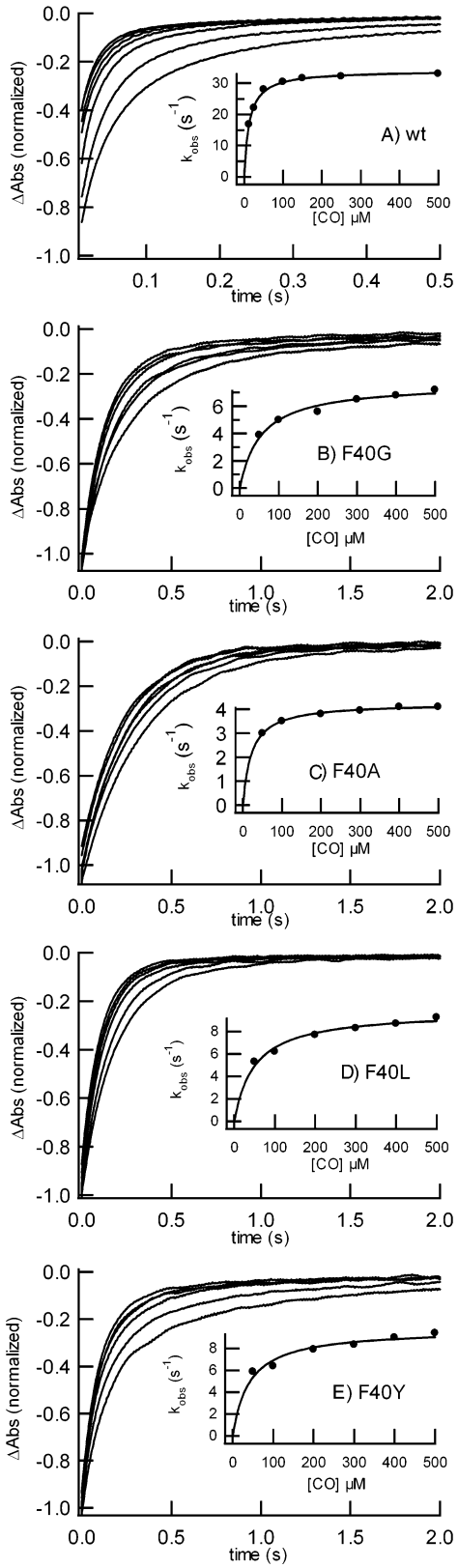

FIGURE 2: CO binding to ferrous riceHb1 and Phe^{B10} mutant proteins. The time courses are measured at different [CO] ranging from 50 to 500 μM (after mixing). The *y*-axes are normalized to the expected ΔAbs for the reaction. Only the wild-type protein shows an observed ΔAbs less than that expected and a decrease in ΔAbs as [CO] is increased. This indicates that the Phe^{B10} mutant proteins have much larger values of K_{H2} than the wild-type protein. Inset: $k'_{CO,obs}$ is plotted versus the [CO] for each protein. The asymptotes in these plots are equal to k_{-H2}.

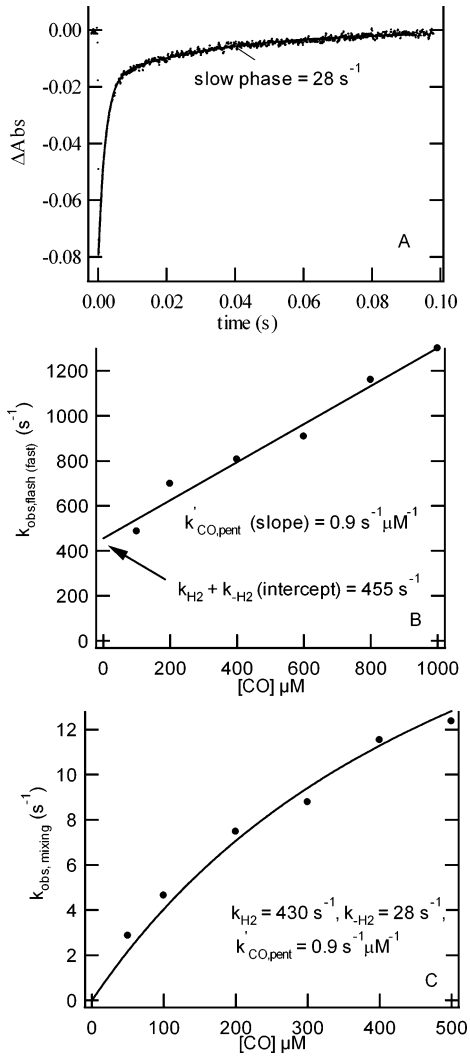

FIGURE 3: CO binding to ferrous F40W. (A) Time course for CO rebinding following flash photolysis is biphasic. The slow phase (28 s^{-1}) is independent of [CO]. (B) [CO] dependence of the faster rate constant, as measured by flash photolysis, provides k'_{CO} and has a *y*-intercept equal to 455 s^{-1}. (C) Rate constants for CO binding following rapid mixing plotted as a function of [CO]. This asymptote is the same as the slow phase in (A).

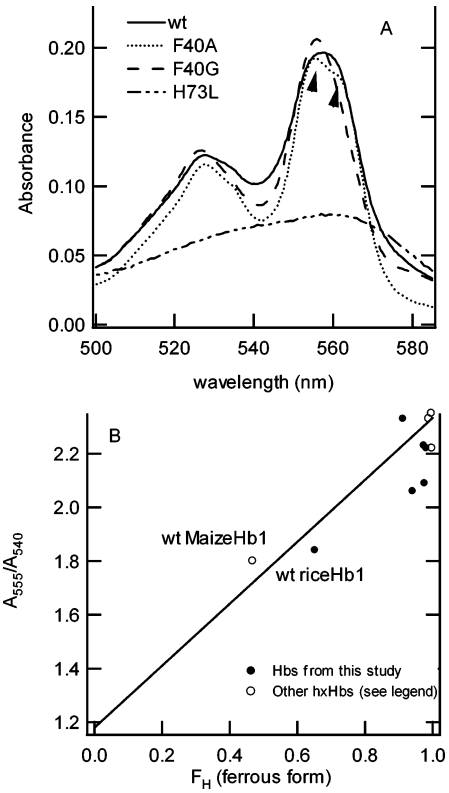

FIGURE 4: Visible absorbance spectra for deoxyferrous riceHb1 and Phe^{B10} mutant proteins. (A) The two peaks associated with these proteins are indicative of hexacoordination and are lacking in the pentacoordinate H73L mutant protein. The arrowheads indicate the bimodal shape of the F40A mutant spectrum. (B) The ratio of absorbance at 555 nm versus 540 nm is plotted against the fraction of hexacoordinate protein (as measured in Figures 2 and 3). The open circles (○) are data taken from Smagghe et al. (*16*), with the plant hxHbs labeled explicitly and the three others (*Synechocystis* Hb, human neuroglobin, and human cytoglobin) grouped in the top right corner). Phe^{B10} mutant proteins are shown as filled circles (●). Each mutant protein has a value of $A_{555}/A_{540} > 2.0$, consistent with F_H values approaching 1 (similar to that of the bacterial and human hxHbs).

complete expected ΔAbs (like the other phe^{B10} mutant proteins) but larger values of $k'_{CO,obs}$ (Figure 3C) (closer to wild-type riceHb1). The slow phase in Figure 3A is consistent with the asymptote in Figure 3C; therefore, this value (28 s^{-1}) has been assigned to k_{-H2}. The value of k_{H2} resulting from the fit of eq 2 to the data in Figure 3C returns a value of 430 s^{-1} for k_{H2}, as expected from the *y*-intercept from flash photolysis (Figure 3B, *y*-intercept (*18*)). The results from Figures 2 and 3 indicate that all Phe^{B10} substitutions have profound effects on K_{H2} and that F40W appears different from the others because of the unusually slow value of k'_{CO}.

As has been described for other hxHbs (*16*, *28*), these changes in K_{H2} should be reflected in visible absorbance spectra. Figure 4A shows a few of these spectra (for clarity) along with that of ferrous H73L riceHb1, which serves as a pentacoordinate reference for $F_H = 0$. The ratio of A_{555}/A_{540} has been shown to correlate with F_H such that when $F_{H2} \sim 1$, the A_{555}/A_{540} ratio is ~2.2 (*16*). The values of F_{H2} that are lower are represented by lower values of A_{555}/A_{540}. The ratios for wild-type riceHb1 and wild-type maizeHb1 indicate values of F_H that are lower than those of hxHbs from humans and bacteria; these values are plotted as open circles (Figure 4B). The points for each of the Phe^{B10} mutant proteins (closed circles) are grouped along with the human and bacterial hxHbs that have larger values of K_{H2} (Figure 4B).

The spectra shown in Figure 4A demonstrate some subtle differences resulting from Phe^{B10} mutation. The F40A spectrum is clearly bimodal (the two peaks indicated by arrowheads), whereas that of the F40G mutant protein is sharper and centered on the lower wavelength mode of the F40A spectrum. The wild-type protein appears to be a symmetric average of the two. These data suggest that the His^{E7} can adopt at least two orientations that are not in fast exchange. These results are consistent with other hexacoordinate hemoglobins (*31*, *32*) and demonstrate that Phe^{B10} can influence the nature of the bond between His^{E7} and the heme iron in plant hxHbs.

Environment of the Ligand-Bound Heme Pocket. Exogenous ligand binding requires the dissociation of the His^{E7} side chain to open a binding site on the heme iron. The only X-ray structure of riceHb1 is in the hexacoordinate state (*33*); therefore, the structural rearrangements accompanying ligand

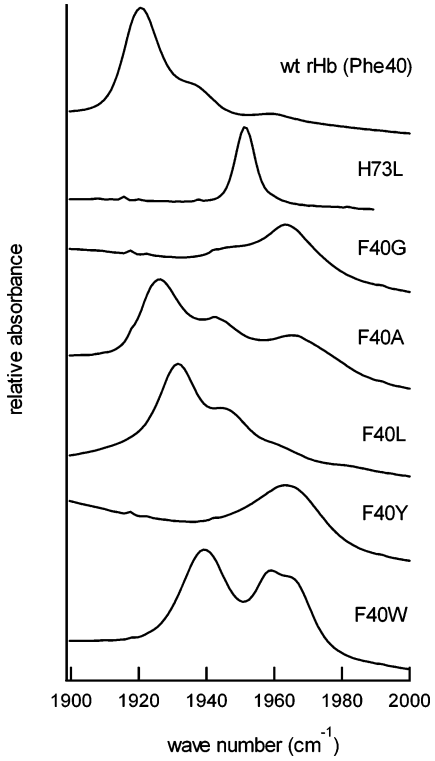

FIGURE 5: CO FTIR absorbance spectra for wild-type riceHb1 and each Phe^{B10} mutant protein. The spectrum of the wild-type protein is indicative of a strong H-bonding interaction between His^{E7} and the CO ligand (*6*). The spectrum of the pentacoordinate H73L mutant protein shifts to a higher energy, suggesting that His^{E7} in the wild-type protein is the major influence on the electrostatic environment around the bound CO. Each Phe^{B10} mutant protein greatly perturbs the spectrum compared to that of the wild-type protein.

binding are currently unknown. However, without any major structural changes, the Phe^{B10} side chain would probably be near the bound ligand. To test the effects of Phe^{B10} substitutions on the structure of the ligand-bound protein, we have used the CO FTIR spectrum as a probe of the electrostatic environment around the bound ligand (Figure 5) (*6*, *34*, *35*). This technique measures the C−O stretching frequency, which is perturbed by the electrostatic charges that are near the bound ligand. A strong positive field (like that associated with a strong hydrogen bond donor) stabilizes the carboxy ligand and shifts the absorbance to a lower frequency, as exemplified by the V68N sperm whale myoglobin mutant protein ($\nu_{Fe-CO} = 1916$ cm^{-1}; (*34*)).

The spectrum of wild-type riceHb1 is indicative of such an interaction, with the major absorbance peak near 1920 cm^{-1}. The fact that the H73L mutant protein lacks this low energy band suggests that the His^{E7} side chain in the wild-type protein is providing the partial positive charge. Similar results have been reported for pentacoordinate plant Hbs (*6*). CO FTIR spectra for each Phe^{B10} mutant protein are compared to those of wild type and H73L riceHb1 in Figure 5. Each spectrum differs from the wild-type protein, indicating major perturbations in the electrostatic environment around the bound CO. The effects of the substitutions are complex, but a common feature of each is a shift in the average ν_{co} value to a higher energy than that of the wild-type protein (Table 1), indicating a weakened hydrogen bond between the His^{E7} side chain and the bound ligand (*5*, *35*).

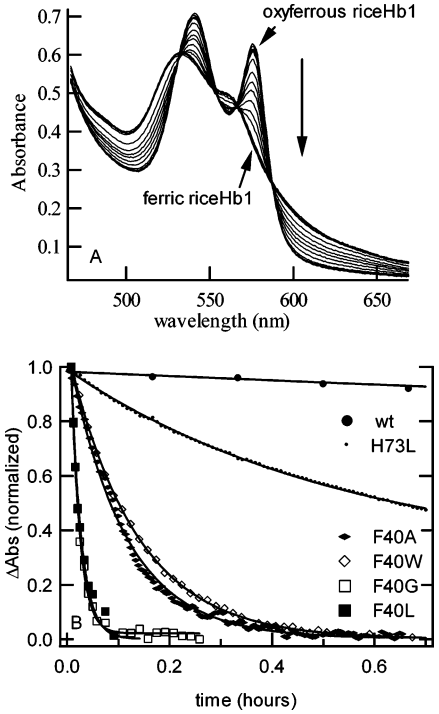

FIGURE 6: Autoxidation measurements. (A) Characteristic visible absorption spectra associated with the autoxidation of wild-type riceHb1. The oxidation of wild type and Phe^{B10} mutant protein was monitored as a decrease in absorbance at 575 nm. (B) The time courses for the autoxidation of each Phe^{B10} mutant protein are much more rapid than that for the wild type or H73L mutant protein.

Oxygen Binding and Autoxidation. Another important reaction that could be affected by Phe^{B10} substitutions is oxygen binding. Wild type riceHb1 binds oxygen with relatively high affinity (*36*). However, efforts to measure rate constants for most Phe^{B10} mutant proteins were met with difficulty. One reason for this might be an effect of the mutation on the stability of the oxyferrous complex, which is dictated by the rate of autoxidation of the heme iron (4). Figure 6A shows the spectral change associated with autoxidation, and Figure 6B demonstrates that the time course (at 575 nm) for oxidation of wild type riceHb1 is relatively slow (Table 1) with a half-life of ∼9 h at 20° C. However, the rate constant for autoxidation is dramatically increased for each Phe^{B10} mutant protein (Figure 6B, Table 1). In fact, only the F40W protein formed an oxyferrous complex stable enough for the measurement of its oxygen dissociation rate constant (k_{O2}). The k_{O2} value for F40W (0.06 s^{-1}) is only slightly faster than that of the wild-type protein (0.038 s^{-1}; Table 1).

Ligand Binding and Hexacoordination in the Ferric Oxidation State

There have been few kinetic measurements of ligand binding to plant hxHbs in the ferric state, presumably because His^{E7} is bound more tightly, resulting in low exogenous ligand affinities and slow reaction time courses. An assumption of the importance of oxygen binding and the convention of the ferrous Hb as the eminent functional form has also contributed to a lack of investigation in this direction. However, it is possible that the ferric oxidation state is important in riceHb1 function (as part of the NO dioxygenation cycle (*9*), for example), and Phe^{B10} could be under

selection pressure for its role in this form of the protein. Therefore, we have investigated the effects of the Phe^{B10} substitutions described above on ligand binding and hexacoordination in the ferric state.

Midpoint Redox Potentials and Ferric Hexacoordination. The midpoint reduction potential of a Hb is a measure of the free energy required to reduce the ferric form of the protein to the ferrous oxidation state. Midpoint potentials for pentacoordinate Hbs such as Mb (+60 mV) (*37*) and plant leghemoglobins (+20 mV) (*38*) have values that are slightly positive with respect that of to a standard hydrogen electrode (SHE), representing reduced states that are thermodynamically more stable than those of hxHbs, which have negative midpoint potentials (typically lower than −100 mV (*28*, *39*)). There are a number of factors that can influence these values (*40*). The thermodynamic linkage between all of the reactions in Scheme 1 indicates that midpoint potentials will be directly influenced by differential coordination of ligands in the ferrous versus the ferric states (*27*). For example, if the His^{E7} side chain coordinates more tightly in the ferric versus the ferrous state, the midpoint potential would be more negative compared to that of a pentacoordinate Hb with all other factors being equal.

Assuming that this shift is due only to the coordination of His^{E7} in the wild-type protein, one can calculate effects of hexacoordination on potentiometric titrations using the following equation (a similar equation is derived by Moore and Pettigrew (*27*)):

$$F_{\text{reduced}} = \frac{e^{-(nF(E_{\text{obs}}-E_{\text{mid}})/RT)}}{\left(\frac{1+K_{\text{H3}}}{1+K_{\text{H2}}}\right)+e^{-(nF(E_{\text{obs}}-E_{\text{mid}})/RT)}} \quad (5)$$

Here, all variables are as described for eq 4 except $F_{\text{reduced}} = (\text{Hb}_{\text{P2}} + \text{Hb}_{\text{H2}})/(\text{Hb}_{\text{P2}} + \text{Hb}_{\text{P3}} + \text{Hb}_{\text{H2}} + \text{Hb}_{\text{H3}})$.

Figure 7A demonstrates the spectral change associated with the potentiometric titration of wild-type riceHb1. Figure 7B shows F_{reduced} as a function of E_{obs} for wild-type riceHb1, H73L, and each Phe^{B10} mutant protein, and the value of E_{mid} for each experiment is listed in Table 2. The H73L mutant protein has been shown to be a pentacoordinate version of riceHb1 (*36*). It has a midpoint potential of −30 mV, whereas the wild-type protein has a value of −143 mV. This indicates that His^{E7} coordination in the wild-type protein is tighter in the ferric versus the ferrous state. Quantification of the ratio of affinity constants is facilitated by the following equation that directly relates the two values to the midpoint potentials for the hxHb ($E_{\text{mid,hex}}$) and the pentacoordinate Hb ($E_{\text{mid,pent}}$).

$$\left(\frac{1+K_{\text{H3}}}{1+K_{H2}}\right) = e^{-(nF(E_{\text{obs}}-E_{\text{mid}})/RT)} \quad (6)$$

Eq 6 demonstrates that if $(1+K_{\text{H3}})/(1+K_{\text{H2}}) > 1$, E_{mid} will shift to a more negative value. Likewise, if $(1+K_{\text{H3}})/(1+K_{\text{H2}}) < 1$, E_{mid} will become more positive.

The ratio of $(1+K_{\text{H3}})/(1+K_{\text{H2}})$ for wild-type riceHb1 is calculated to be 80 (Table 2), indicating that hexacoordination is much tighter in the ferric than in the ferrous state. For each Phe^{B10} mutant protein, the value of E_{mid} is shifted to a more negative value, and the $(1+K_{\text{H3}})/(1+K_{\text{H2}})$ ratios are higher compared to the wild-type protein (Table 2),

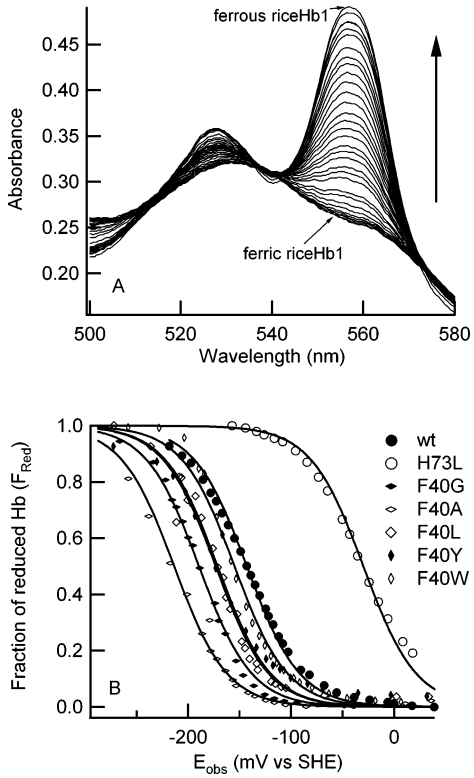

FIGURE 7: Potentiometric titration experiments. (A) The absorption spectra associated with the reduction of ferric riceHb1; the fraction of reduced protein was measured at 557 nm. (B) The reduction potential for each protein (E_{obs}) is measured by sodium dithionite titration under anaerobic conditions and is plotted vs the fraction of reduced protein (F_{red}). The solid lines are fits to eq 4 with E_{mid} as the fitted parameter. The H73L mutant protein has a value of E_{mid} that is shifted by +113 mV compared to the wild-type protein, and each Phe^{B10} mutant protein shifts the value of E_{mid} to a more negative one.

Table 2: Reduction Potentials and Azide Binding

protein	E_{Mid} (mV)	$(1+K_{\text{H3}})/(1+K_{\text{H2}})$	$K_{\text{obs,azide}}$ (mM^{-1})
H73L	−30		0.45
F40G	−189	490	<0.0002
F40A	−214	1300	0.0006
F40L	−173	260	0.25
Phe^{40} (wt)	−143	80	1.6
F40Y	−171	240	0.002
F40W	−155	130	0.0003

indicating that Phe^{B10} is the most successful at inhibiting hexacoordination in the ferric state relative to the ferrous state.

Azide Binding. The reduction potentials measured above suggest that Phe^{B10} substitutions should lower the affinity for exogenous ligands in the ferric state compared to wild-type riceHb1 because of the increased competition for the binding site by the His^{E7} side chain. In general, the effect of hexacoordination on exogenous ligand binding can be calculated by the following equation, where K_{pent} is the ligand association equilibrium constant in the absence of hexacoordination (*20*):

$$K_{\text{obs}} = \frac{K_{\text{pent}}}{1+K_{\text{H}}} \quad (7)$$

All of the Phe^{B10} mutations increase both K_{H2} and the

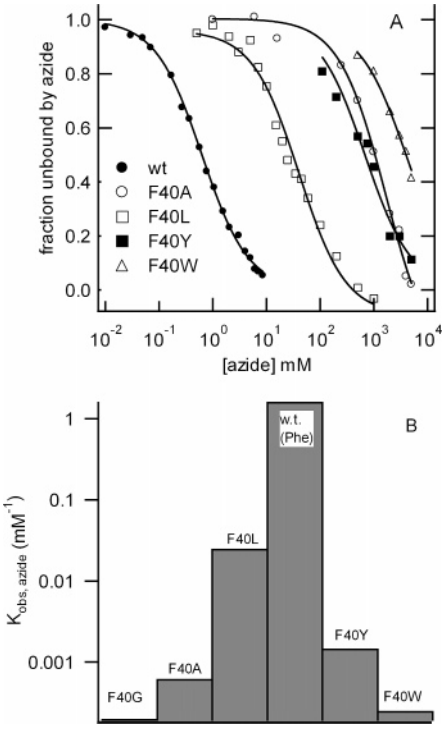

FIGURE 8: Azide binding to ferric riceHb1 and Phe^{B10} mutant proteins. (A) Azide titration curves for each protein; the solid lines are fits to eq 3. (B) Association equilibrium constants for azide for wild-type riceHb1 and each Phe^{B10} mutant protein as measured in A. The wild-type protein has by far the largest affinity for azide.

$(1+K_{H3})/(1+K_{H2})$ ratio. Therefore, each mutant protein must have a very large absolute value of K_{H3} compared to that of the wild-type protein and thus a lower K_{obs} for exogenous ferric ligands.

To test this prediction we have measured azide binding to each protein by equilibrium titration as shown in Figure 8. For each mutant protein, the association equilibrium constant decreases dramatically (Figure 8B, Table 2). The wild-type protein has a higher affinity for azide by at least 60-fold (and on average 3000-fold) compared to each Phe^{B10} mutant protein.

X-ray Crystallography of Ferric Phe^{B10} Mutant Proteins. In an effort to better understand the effects of Phe^{B10} substitution, the X-ray crystal structures of the ferric forms of the F40L and F40W mutant proteins have been solved (Figure 9). There are no major structural perturbations resulting from these substitutions compared to the structure of wild-type riceHb1. However, subtle changes in the heme pocket are observed. Figure 9A demonstrates that Phe^{B10} in wild-type riceHb1 packs against His^{E7} and, along with Val^{E11} and Phe^{CD1}, likely blocks major movement or rotation. The F40L substitution creates a cavity above the His^{E7} side chain and allows it to rotate in that direction. However, the Trp^{B10} side chain of the F40W mutant protein forces His^{E7} to rotate in the opposite direction (Figure 9B).

Each of these structures has two molecules in the asymmetric unit (Figure 9C). The two molecules are similar for the wild type and F40L proteins, but the F40W structure shows two very different conformations for the Trp^{B10} side chain. One molecule of the asymmetric unit is as shown in Figure 9B. In the other, the Trp^{B10} side chain moves out of the heme pocket and creates a cavity similar to that in the structure of the F40L protein. The His^{E7} side chain rotates toward this cavity in the B molecule of the F40W structure as well (Figure 9C). The two locations observed for Trp^{B10} might also be responsible for the two His^{E7} conformations in the CO form of the protein (two major IR peaks, Figure 5).

DISCUSSION

Studies of Hbs from different organisms have revealed the importance of the amino acids at positions E7 and B10 for directing the chemistry of the heme pocket and the function of the protein. In human oxygen transport globins (Leu at B10) and leghemoglobins (Tyr/Phe at B10), the B10 side chain regulates ligand binding by affecting the position and reactivity of His^{E7} (*3*, *5*, *6*, *41*). In bacteria, the Tyr^{B10} side chain interacts directly with the bound ligand (*10*). The results presented here show that the conserved Phe^{B10} found in plant hxHbs affects hexacoordination in both the ferrous and the ferric oxidation states and has a profound influence on the rate constants for autoxidation. These results are discussed below in the context of their impact on Hb structure and function and the potential physiological function of plant Hbs.

Phe^{B10} Directs the Action of His^{E7}. The conserved tertiary structure of the globin fold forces certain amino acids to exist near one another. Throughout the evolution of Hbs, this has been the case for the B10 and E7 side chains. The combination of Tyr^{B10}/Gln^{E7} common in bacteria is good for scavenging oxygen by using the Tyr side chain as the principle source of stabilization. Oxygen transport apparently requires different regulation and a lower affinity constant than is attainable through stabilization using the combination of Tyr^{B10}/Gln^{E7}. His^{E7} takes the spotlight for this purpose, and the side chain at B10 has been relegated to a supporting role. For example, hemoglobin 1 from *Lucina pectinata* (Gln^{E7}/Phe^{B10}) has a very fast oxygen off rate, suggesting weak stabilization of the bound ligand. However, replacing the E7 by a His or the B10 by a Tyr lowers the oxygen off rate by a factor 50 and 250, respectively suggesting the important roles of these two amino acid in ligand stabilization (*42*). The reason for His^{E7} instead of Gln^{E7} in oxygen transport is probably due to the fact that the Gln side chain has more degrees of rotational freedom and is a weaker hydrogen bond donor (*35*, *43*). Therefore, it is statistically less likely that the Gln side chain will adopt a thermodynamically favorable conformation for hydrogen bonding with bound oxygen. For this reason, most oxygen transport Hbs have His^{E7} held in just the right orientation through steric interactions with an aliphatic or Phe side chain at position B10 (*6*).

In addition to stabilizing bound ligands, His^{E7} in hxHbs is also capable of reversible coordination of the ligand binding site on the heme iron. This coordination is very important for the stability of the protein (*44*) and can be influenced by the physical and chemical environment surrounding the coordinating His side chain (*45*). Given the partnership between these amino acids in pentacoordinate Hbs, it is not surprising that the B10 amino acid is also important in hxHbs. More surprising are the specific effects of the Phe^{B10} side chain in riceHb1. Without Phe at this position, hexacoordination is greatly enhanced, shifting the behavior of the protein in the direction of bacterial and animal hxHbs.

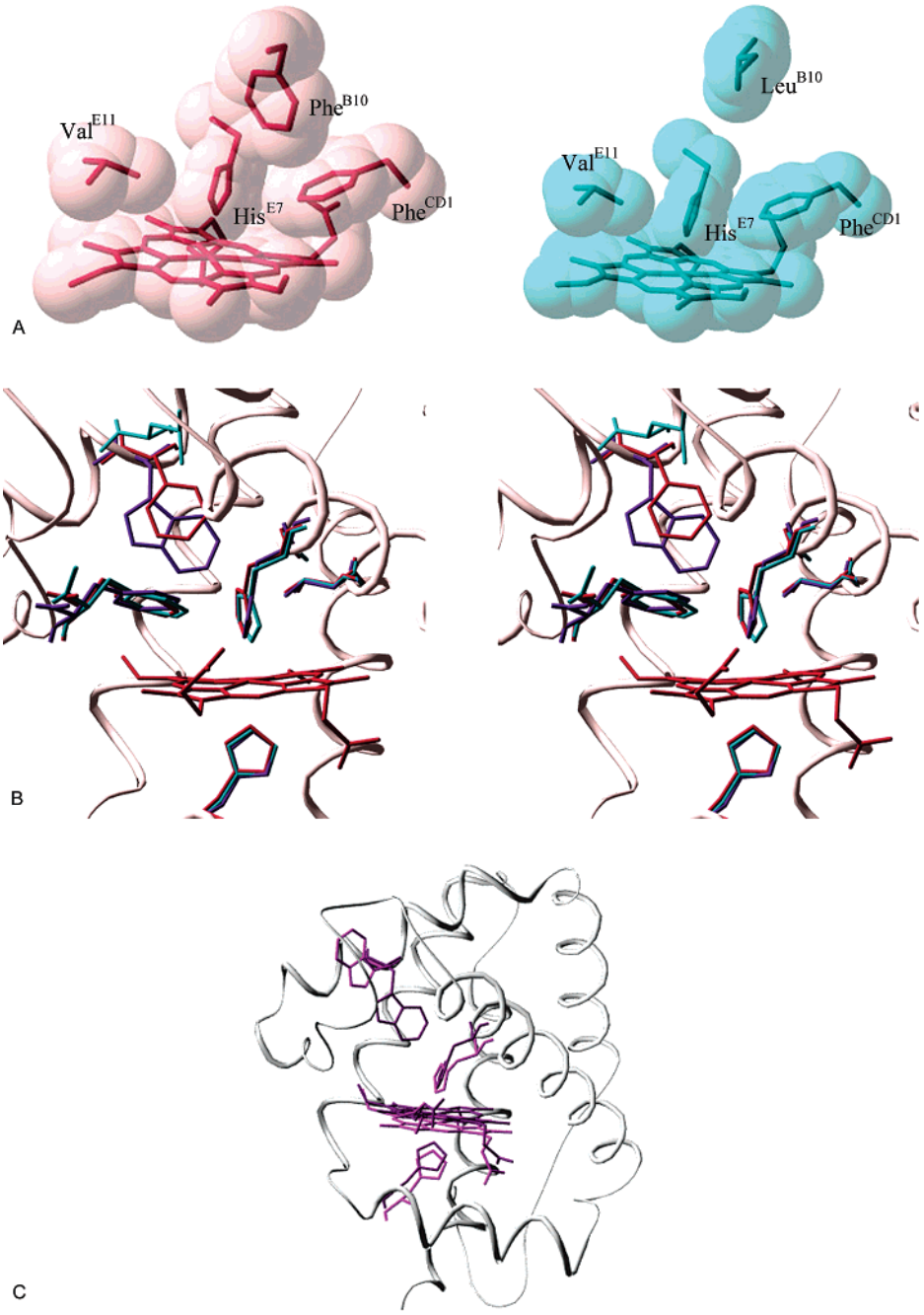

FIGURE 9: X-ray crystal structures of ferric, hexacoordinate F40L, and F40W riceHb1 compared to that of the wild-type protein. (A) A space filling model of wild-type riceHb1 (left) shows that Phe^{B10}, Phe^{CD1}, and Val^{E11} pack tightly against the coordinating His^{E7} side chain. The F40L protein (right) creates a cavity near the His^{E7} side chain. (B) The structures of F40L (blue) and F40W (chain A, purple) are overlaid with wild-type riceHb1 (red). His^{E7} rotates in opposite directions in each mutant protein compared to its position in wild-type riceHb1. (C) An overlay of the two molecules in the asymmetric unit of the F40W mutant protein shows two conformations for the Phe^{40} side chain.

In the hexacoordinate conformation, Phe^{B10} interacts with His^{E7} just enough to stimulate dissociation but not enough to prevent coordination. This conclusion is supported by the dramatic effect of Phe^{B10} substitution on K_{H2}, K_{H3}, and $(1+K_{H3})/(1+K_{H2})$. Once an exogenous ligand (like oxygen) is bound, Phe^{B10} forces the His^{E7} side chain to move only to a position from which it can form a stabilizing hydrogen bond. This conclusion is supported by the CO−FTIR spectra of Phe^{B10} mutant proteins showing greater movement of the His^{E7} side chain within the distal heme pocket in the absence of Phe at this position. The large increase in autoxidation upon B10 mutation is probably a consequence of the inability of His^{E7} to form a strong hydrogen bond with bound oxygen, in combination with solvent entry into the distal heme pocket (*4*, *46*). Finally, it is clear from the phylogenetic conservation of Phe^{B10} in the nsHbs that these functions are likely critical to the physiological role of this class of proteins.

Oxygen Transport versus NO Scavenging. Two possible functions for nsHbs are oxygen transport and NO detoxification. The likelihood of the former possibility is diminished by low Hb concentrations and the slow kinetics of oxygen release. The possibility of the latter is strong but difficult to test because any oxyHb will destroy NO in a test tube (9). Recent experiments demonstrating this capacity explicitly

in oxy-nsHbs confirm that they destroy NO like many others (*47*, *48*). However, Hbs are poor NO scavengers in the absence of mechanisms for heme rereduction (as observed for the flavohemoglobins (*13*, *14*, *49*)), and no reductase has yet been identified for any other Hb for which NO scavenging has been proposed as a principal physiological function (*8*, *48*, *50*, *51*). Without identification of a reduction mechanism, the identification of NO dioxygenation as a function for Hbs is premature (*21*, *52*−*54*).

It is reported here that the conservation of Phe^{B10} in nsHbs is important for stabilization of the oxy-ferrous complex. This would obviously favor a role in oxygen transport. However, it would also favor NO scavenging because oxyHb is the principal reactant in NO dioxygenation. Therefore, although we have learned the effect of Phe^{B10} on the chemistry of nsHbs, we cannot use this information to distinguish between the potential functions of oxygen transport and NO scavenging. However, we can differentiate between nsHb and other hxHbs; the slower autoxidation and lower hexacoordination affinity constants conferred by Phe^{B10} are not shared by neuroglobin, cytoglobin, or *Synechocystis* Hb (*16*).

Significance of Reactions with Ferric hxHbs. Phe^{B10} prevents tight His^{E7} coordination in the ferric state, thus facilitating ligand binding by removing competition for the binding site. This allows ferric riceHb1 to bind ligands with submillimolar affinity. The potential importance of ligand binding in the ferric oxidation state has been greatly overlooked, but some recent work has focused on this possibility. A good example is found in *Arabidopsis*, where the three ferric hemoglobins show a peroxidase-like activity (*55*).

In conclusion, the results presented here demonstrate the importance of Phe at the B10 position in plant hxHbs and suggest that reactions with ferric ligands should be considered because they might reflect potentially important functions. Our consideration of protein function underlines the intertwined chemical relationship between oxygen binding and NO dioxygenation that precludes the identification of either of the two as a physiological function based solely on the ability of a Hb to facilitate these reactions in vitro.

ACKNOWLEDGMENT

We thank Mario Rivera and Adriana Altuve for advice on building our potentiometric titration apparatus and John S. Olson and George C. Blouin for help with IR spectroscopy.

REFERENCES

1. Antonini, E., and Brunori, M. (1971) *Hemoglobin and Myoglobin in their Reactions with Ligands*, Vol. 21, North-Holland Publishing Company, Amsterdam, The Netherlands.
2. Olson, J. S., and Phillips, G. N., Jr. (1997) Myoglobin discriminates between O_2, NO, and CO by electrostatic interactions with the bound ligand, *J. Biol. Inorg. Chem. 2*, 544−552.
3. Carver, T. E., Brantley, R. E., Jr., Singleton, E. W., Arduini, R. M., Quillin, M. L., Phillips, G. N., Jr., and Olson, J. S. (1992) A novel site-directed mutant of myoglobin with an unusually high O2 affinity and low autooxidation rate, *J. Biol. Chem. 267*, 14443−14450.
4. Brantley, R. E., Jr., Smerdon, S. J., Wilkinson, A. J., Singleton, E. W., and Olson, J. S. (1993) The mechanism of autooxidation of myoglobin, *J. Biol. Chem. 268*, 6995−7010.
5. Kundu, S., and Hargrove, M. S. (2003) Distal heme pocket regulation of ligand binding and stability in soybean leghemoglobin, *Proteins 50*, 239−248.
6. Kundu, S., Blouin, G. C., Premer, S. A., Sarath, G., Olson, J. S., and Hargrove, M. S. (2004) TyrB10 inhibits stabilization of bound oxygen in soybean leghemoglobin, *Biochemistry 43*, 6241−6252.
7. Wittenberg, J. B., Bolognesi, M., Wittenberg, B. A., and Guertin, M. (2002) Truncated hemoglobins: a new family of hemoglobins widely distributed in bacteria, unicellular eukaryotes, and plants, *J. Biol.* Chem. *277*, 871−874.
8. Hankeln, T., Ebner, B., Fuchs, C., Gerlach, F., Haberkamp, M., Laufs, T. L., Roesner, A., Schmidt, M., Weich, B., and Wystub, S. (2005) Neuroglobin and cytoglobin in search of their role in the vertebrate globin family, *J. Inorg. Biochem. 99*, 110−119.
9. Kundu, S., Trent, J. T., III, and Hargrove, M. S. (2003) Plants, humans and hemoglobins, *Trends Plant Sci. 8*, 387−393.
10. Milani, M., Pesce, A., Nardini, M., Ouellet, H., Ouellet, Y., Dewilde, S., Bocedi, A., Ascenzi, P., Guertin, M., and Moens, L. (2005) Structural bases for heme binding and diatomic ligand recognition in truncated hemoglobins, *J. Inorg. Biochem. 99*, 97−109.
11. Bolognesi, M., Bordo, D., Rizzi, M., Tarricone, C., and Ascenzi, P. (1997) Nonvertebrate hemoglobins: structural bases for reactivity, *Prog. Biophys. Mol. Biol. 68*, 29−68.
12. Pietri, R., Granell, L., Cruz, A., De Jesus, W., Lewis, A., Leon, R., Cadilla, C., and Garriga, J. (2005) Tyrosine B10 and heme-ligand interactions of Lucina pectinata hemoglobin II: control of heme reactivity, *Biochim. Biophys. Acta 1747*, 195−203.
13. Gardner, A. M., Martin, L. A., Gardner, P. R., Dou, Y., and Olson, J. S. (2000) Steady-state and transient kinetics of *Escherichia coli* nitric-oxide dioxygenase (flavohemoglobin). The B10 tyrosine hydroxyl is essential for dioxygen binding and catalysis, *J. Biol. Chem. 275*, 12581−12589.
14. Gardner, P. R., Gardner, A. M., Martin, L. A., and Salzman, A. L. (1998) Nitric oxide dioxygenase: an enzymatic function for flavohemoglobin, *Proc. Natl. Acad. Sci. U.S.A. 95*, 10378−10383.
15. Hargrove, M. S., Brucker, E. A., Stec, B., Sarath, G., Arredondo-Peter, R., Klucas, R. V., Olson, J. S., and Phillips, J., George N. (2000) Crystal structure of a nonsymbiotic plant hemoglobin, *Structure 8*, 1005−1014.
16. Smagghe, B. J., Sarath, G., Ross, E., Hilbert, J.-l., and Hargrove, M. S. (2006) Slow ligand binding kinetics dominate ferrous hexacoordinate hemoglobin reactivities and reveal differences between plants and other species, *Biochemistry 45*, 561−570.
17. Trent, J. T., III, Hvitved, A. N., and Hargrove, M. S. (2001) A model for ligand binding to hexacoordinate hemoglobins, *Biochemistry 40*, 6155−6163.
18. Hargrove, M. S. (2000) A flash photolysis method to characterize hexacoordinate hemoglobin kinetics, *Biophys. J. 79*, 2733−2738.
19. Olson, J. S. (1981) Stopped-flow, rapid mixing measurements of ligand binding to hemoglobin and red cells, *Methods Enzymol. 76*, 631−651.
20. Trent, J. T., III, Watts, R. A., and Hargrove, M. S. (2001) Human neuroglobin, a hexacoordinate hemoglobin that reversibly binds oxygen, *J. Biol. Chem. 276*, 30106−30110.
21. Weiland, T. R., Kundu, S., Trent, J. T., III, Hoy, J. A., and Hargrove, M. S. (2004) Bis-histidyl hexacoordination in hemoglobins facilitates heme reduction kinetics, *J. Am. Chem. Soc. 126*, 11930−11935.
22. Altuve, A., Wang, L., Benson, D., and Rivera, M. (2004) Mammalian mitochondrial and microsomal cytochromes b(5) exhibit divergent structural and biophysical characteristics, *Biochem. Biophys. Res. Commun. 314*, 602−609.
23. Pflugrath, J. (1999) The finer things in X-ray diffraction data collection, *Acta Crystallogr., Sect. D 55*, 1718−1725.
24. Brunger. (1998) Crystallography & NMR System, *Acta Crystallogr. D54*, 901−921.
25. Number, C. C. P. (1994) The CCP4 suite: programs for protein crystallography, *Acta Crystallogr., Sect. D 50*, 760−763.
26. Jones, T., Zou, J., and Kjeelgaard, M. (1991) Improved methods for building protein models in electron-density maps and location of errors in these models, *Acta Crystallogr., Sect. A 47*, 110−119.
27. Moore, G., and Pettigrew, G. (1990) *Cytochromes c: Evolutionary, Structural and Physicochemical Aspects*, Springer, Berlin.
28. Dewilde, S., Kiger, L., Burmester, T., Hankeln, T., Baudin-Creuza, V., Aerts, T., Marden, M. C., Caubergs, R., and Moens, L. (2001) Biochemical characterization and ligand binding properties of neuroglobin, a novel member of the globin family, *J. Biol. Chem. 276*, 38949−38955.
29. Couture, M., Das, T. K., Savard, P.-Y., Ouellet, Y., Wittenberg, J. B., Wittenberg, B. A., Rousseau, D. L., and Guertin, M. (2000)

Structural investigations of the hemoglobin of the cyanobacterium Synechocystis PCC6803 reveal a unique distal heme pocket, *Eur. J. Biochem. 267*, 4770−4780.
30. Trent, J. T., III, Kundu, S., Hoy, J. A., and Hargrove, M. S. (2004) Crystallographic analysis of Synechocystis cyanoglobin reveals the structural changes accompanying ligand binding in a hexacoordinate hemoglobin, *J. Mol. Biol. 341*, 1097−1108.
31. Duff, S. M. G., Wittenberg, J. B., and Hill, R. D. (1997) Expression, purification, and properties of recombinant barley (*Hordeum* sp.) hemoglobin, *J. Biol. Chem. 272*, 16746−16752.
32. Hvitved, A. N., Trent, J. T., III, Premer, S. A., and Hargrove, M. S. (2001) Ligand binding and hexacoordination in *Synechocystis* hemoglobin, *J. Biol. Chem. 276*, 34714−34721.
33. Hargrove, M., Brucker, E., Stec, B., Sarath, G., Arredondo-Peter, R., Klucas, R., Olson, J., and Phillips, G. (2000) Crystal structure of a nonsymbiotic plant hemoglobin, *Structure Fold. Des. 8*, 1005−1014.
34. Phillips, G. N. J., Teodoro, M. L., Li, T., Smith, B., and Olson, J. S. (1999) Bound CO is a molecular probe of electrostatic potential in the distal pocket of myoglobin, *J. Phys. Chem. B 103*, 8817−8829.
35. Li, T., Quillin, M. L., Phillips, G. N., Jr., and Olson, J. S. (1994) Structural determinants of the stretching frequency of CO bound to myoglobin, *Biochemistry 33*, 1433−1446.
36. Arredondo-Peter, R., Hargrove, M. S., Sarath, G., Moran, J. F., Lohrman, J., Olson, J. S., and Klucas, R. V. (1997) Rice hemoglobins. Gene cloning, analysis, and O_2-binding kinetics of a recombinant protein synthesized in *Escherichia coli*, *Plant Physiol. 115*, 1259−1266.
37. Brunori, M., Saggese, U., Rotilio, G., Antonini, E., and Wyman, J. (1971) Redox equilibrium of sperm-whale myoglobin, Aplysia myoglobin, and *Chironomus thummi* hemoglobin, *Biochemistry 10*, 1604−1609.
38. Patel, N., Seward, H., Svensson, A., Gurman, S., Thomson, A., and Raven, E. (2003) Exploiting the conformational flexibility of leghemoglobin: a framework for examination of heme protein axial ligation, *Arch. Biochem. Biophys. 418*, 197−204.
39. LeComte, J., Scott, N., Vu, B., and Falzone, C. (2001) Binding of ferric heme by the recombinant globin from cyanobacterium *Synechocystis* sp. PCC 6803, *Biochemistry 40*, 6541−6552.
40. Mauk, A. G., and Moore, G. R. (1997) Control of metalloprotein redox potentials: what does site-directed mutagenesis of hemoproteins tell us? *J. Biol. Inorg. Chem. 2*, 119−125.
41. Wiltrout, M. E., Giovannelli, J. L., Simplaceanu, V., Lukin, J. A., Ho, N. T., and Ho, C. (2005) A biophysical investigation of recombinant hemoglobins with aromatic B10 mutations in the distal heme pockets, *Biochemistry 44*, 7207−7217.
42. Pietri, R., Leon, R. G., Kiger, L., Marden, M. C., Granell, L. B., Cadilla, C. L., and Lopez-Garriga, J. (2006) Hemoglobin I from Lucina pectinata: A model for distal heme-ligand control, *Biochim. Biophys. Acta 1764*, 758−765.
43. Springer, B. A., Sligar, S. G., Olson, J. S., and Phillips, G. N., Jr. (1994) Mechanisms of ligand recognition in myoglobin, *Chem. Rev. 94*, 699−714.
44. Hamdane, D., Kiger, L., Hoa, G. H. B., Dewilde, S., Uzan, J., Burmester, T., Hankeln, T., Moens, L., and Marden, M. C. (2005) High pressure enhances hexacoordination in neuroglobin and other globins, *J. Biol. Chem. 280*, 36809−36814.
45. Hamdane, D., Kiger, L., Dewilde, S., Uzan, J., Burmester, T., Hankeln, T., Moens, L., and Marden, M. C. (2005) Hyperthermal stability of neuroglobin and cytoglobin, *FEBS J. 272*, 2076−2084.
46. Liong, E., Dou, Y., Scott, E., Olson, J., and Phillips, G., Jr. (2001) Waterproofing the heme pocket. Role of proximal amino acid side chains in preventing hemin loss from myoglobin, *J. Biol. Chem. 276*, 9093−9100.
47. Perazzolli, M., Dominici, P., Romero-Puertas, M., Zago, E., Zeier, J., Sonoda, M., Lamb, C., and Delledonne, M. (2004) Arabidopsis nonsymbiotic hemoglobin AHb1 modulates nitric oxide bioactivity, *Plant Cell 10*, 2785−2794.
48. Perazzolli, M., Romero-Puertas, M. C., and Delledonne, M. (2006) Modulation of nitric oxide bioactivity by plant haemoglobins, *J. Exp. Bot. 57*, 479−488.
49. Gardner, A. M., and Gardner, P. R. (2002) Flavohemoglobin detoxifies nitric oxide in aerobic, but not anaerobic, *Eschericia coli*, *J. Biol. Chem. 277*, 8166−8171.
50. Minning, D., Gow, A., Bonaventura, J., Braun, R., Dewhirst, M., Goldberg, D., and Stamler, J. (1999) *Ascaris* haemoglobin is a nitric oxide-activated 'deoxygenase', *Nature 401*, 497−502.
51. Ouellet, H., Ouellet, Y., Richard, C., Labarre, M., Wittenberg, B., Wittenberg, J., and Guertin, M. (2002) Truncated hemoglobin HbN protects *Mycobacterium bovis* from nitric oxide *Proc. Natl. Acad. Sci. U.S.A. 99*, 5902−5907.
52. Igamberdiev, A., Bykova, N., and Hill, R. (2006) Nitric oxide scavenging by barley hemoglobin is facilitated by a monodehydroascorbate reductase-mediated ascorbate reduction of methemoglobin, *Planta 223*, 1033−1040.
53. Igamberdiev, A. U., Seregelyes, C., Manac'h, N., and Hill, R. D. (2004) NADH-dependent metabolism of nitric oxide in alfalfa root cultures expressing barley hemoglobin, *Planta 219*, 95−102.
54. Brunori, M., Giuffre, A., Nienhaus, K., Nienhaus, G. U., Scandurra, F. M., and Vallone, B. (2005) Neuroglobin, nitric oxide, and oxygen: Functional pathways and conformational changes, *Proc. Natl. Acad. Sci. USA 102*, 8483−8488.
55. Sakamotoa, A., Sakuraob, S., Fukunagab, K., Matsubarac, T., Ueda-Hashimotoa, M., Tsukamotoa, S., Takahashi, M., and Morikawa, H. (2004) Three distinct Arabidopsis hemoglobins exhibit peroxidase-like activity and differentially mediate nitrite-dependent protein nitration, *FEBS Lett. 572*, 27−32.

BI060716S